Oriented Differences of Boxes Operators for Blood Vessel Segmentation and Analysis in Confocal Laser Endomicroscopy Images with minimal User Interaction

Herbert Süße[1]
herbert.suesse@uni-jena.de
Wolfgang Ortmann[1]
wolfgang.ortmann@uni-jena.de
Christian Lautenschläger[2]
christian.lautenschlaeger@med.uni-jena.de
Marco Körner[1]
marco.koerner@uni-jena.de
Carsten Schmidt[2]
carsten.schmidt@med.uni-jena.de
Andreas Stallmach[2]
andreas.stallmach@med.uni-jena.de
Joachim Denzler[1]
joachim.denzler@uni-jena.de

[1] Computer Vision Group
Friedrich Schiller University of Jena
Ernst-Abbe-Platz 3
Jena, Germany

[2] Clinic of Internal Medicine II
University Clinic Jena
Erlanger Allee 101
Jena, Germany

Abstract

Despite of an increasing use of *Confocal Laser Endomicroscopy (CLE)* in gastroenterology, an objective interpretation of this data is not established and its processing still states a very difficult task due to the high amount of noise and motion blur shown in these images. Nevertheless, this imaging technique offers great opportunities in terms of immediate *in vivo* diagnosis of histological alterations, *e.g.* in the case of cancer detection. We present a new framework for joint segmentation, detection, and analysis of vessel structures in CLE images requiring a minimal amount of user feedback. For this purpose we introduce a new type of non-linear derivative operators, the *Oriented Differences of Boxes (ODoB)* filter.

1 Introduction & Related Work

Endomicroscopic imaging has emerged to an established tool in gastrointestinal endoscopy and allows to visualize microscopic alterations of the mucosa during an ongoing endoscopic examination in order to improve diagnosis and to guide therapy. Recently, the representation of mucosal vascularization has attracted substantial scientific interest as it contributes to the pathogenesis of different diseases, such as gastrointestinal cancer and chronic inflammation.

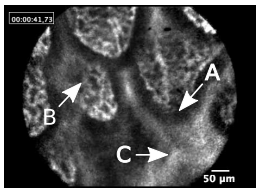

(a) CLE image of non-pathological porcine *ileum*.

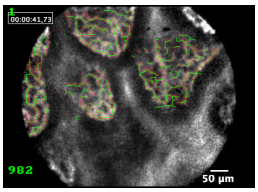

(b) Processed image with segmented vessels (best seen in colors).

Figure 1: (a) CLE images are likely to be corrupted by pixel noise (A), blur (B), and intestinal contents (C). (b) Desired result after processing.

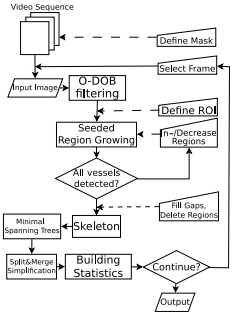

Figure 2: Outline of our framework: dashed and solid lines attached to trapezoids indicate optional and mandatory user interaction, respectively.

However, the images obtained by *Confocal Laser Endomicroscopy (CLE)* imaging are inherently corrupted by noise, blur, low contrast, and other types of disruptions, as exemplarily shown in Fig. 3(a).

Traditionally, CLE images have to be evaluated manually, which is very time-consuming and prone to errors. Hence, vessel segmentation in 2d as well as 3d data is in focus of scientific research for many years, as indicated by literature surveys[2, 3]. While the majority of these methods concentrate on retinal images with reasonable high resolutions and good contrast, only a few approaches exist for noisy CLE images at low resolution. Contrary to us, a remarkable group of approaches propose to use learning-based techniques. Socher *et al*. [6] identifies pixels from retinal images as ridges to get an approximation of the vessel centerlines. Xu *et al*. [7] classifies the output of adaptive local thresholding using SVM. The local geometric structure around vessel pixels is measured by evaluating the corresponding structure tensor by Zheng *et al*. [8]. Another approach more related to our proposal was presented by Rouchdy *et al*. [5] who identifies endpoints of vessels and measures their geodesic distance in order to find optimal connecting paths.

We propose a new framework for semi-automatic processing of CLE images. The amount of user interaction is minimized to a few simple tasks. The remainder is structured as follows: in Sect. 2 we describe the central steps of our approach as displayed in Fig. 2. Afterwards, Sect. 3 gives a brief insight into the subsequent analysis of the segmentation results. In Sect. 4, we discuss the performance of our framework to summarize and conclude in Sect. 5.

2 Preprocessing & Segmentation

2.1 Oriented DoB Filters for Local Structure Enhancement

Since the input images show a high amount of noise and are corrupted by blur—as exemplarily shown in Fig. 1(a)—, preprocessing by non-linear bandpass filtering is mandatory before segmenting vessel candidates. Following, will introduce *Oriented Differences of Boxes (ODoB)* filters and further processing for segmentation of prospective vessel structures. In order to suppress noise in non-vessel regions and simultaneously emphasize the vessel structures themselves, we propose an gradient orientation-specific extension of *Differences of Boxes (DoB)* filter.

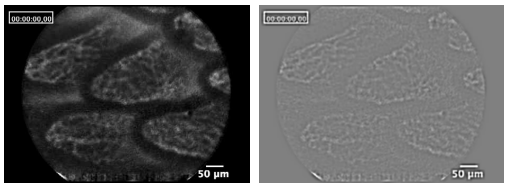

(a) (b)

Figure 3: (a) an input image and (b) the result of traditional non-oriented DoB filtering. The vessel structure is corrupted and noise is not suppressed sufficiently.

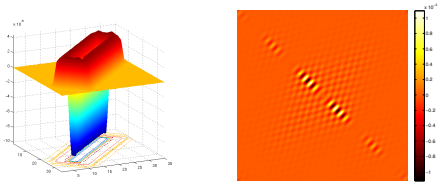

(a) (b)

Figure 4: ODoB Filter for gradient orientation $\varphi = 45°$: (a) in the spatial domain and (b) in the frequency domain. This realizes a complex bandpass filter.

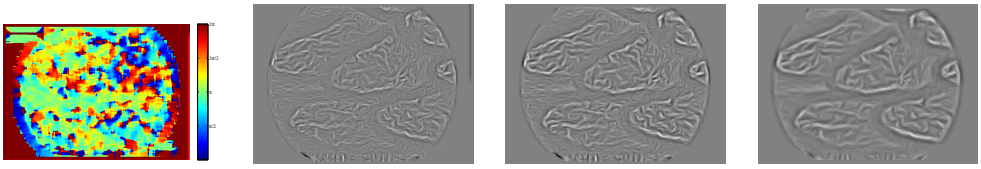

(a) gradient orientations (b) small size (c) medium size (d) large size

Figure 5: Exemplary results of ODoB-filtering image Fig. 3(a): (a) gradient orientations (color coded; best seen in the electronical version), (b)–(d) results for increasing filter sizes. Local vessel structure is drastically enhanced by this operation, while noise and blur is suppressed.

As presented by Rodner *et al.* [4], DoB filters $DoB_{m,M}(g) = \frac{1}{m}\sum_{i=1}^{m} g_i - \frac{1}{M}\sum_{l=1}^{M} g_l$ for 1-dimensional signals g were designed to approximate *Difference of Gaussians (DoG)* or *Laplacian of Gaussian (LoG)* operators usually employed to determine local structure information in a fast and efficient way. Prior knowledge about the target structure can be incorporated by choosing appropriate values for the parameters m and M representing the widths of the outer and the inner box filters, respectively.

Regarding 2d images, this approximation of isotropic LoG operators would destroy structure information, as can be seen in Fig. 3. Therefore, we extend the original DoB filter to align with the local structure tensor—which turns it into a non-linear filter—and call it *Oriented Differences of Boxes (ODoB)* filter. Fig. 4(a) shows a ODoB filter mask oriented by $\varphi = 45°$, while its corresponding power spectrum in frequency domain is illustrated in Fig. 4(b). It gets evident, that this filter realize a complex bandpass filter favoring a certain direction and simultaneously suppressing its orthogonal counterpart. Following this idea, vessel structure will be smoothed along the local gradient direction (*cf.* Fig. 5(a)) and thus emphasized by approximating the local derivatives as shown in Fig. 4 (b)–(d).

2.2 Foreground Segmentation and Vessel Detection

The ODoB-filtered images show enhanced structures with more homogeneous intensities. In order to detect connected areas within the vessels, we apply a parameter-free *Seeded Region Growing (SRG)*[1] algorithm on these images which does not require predefined homogeneity criteria and thresholds. This returns a binary foreground-*vs.*-background segmentation of the input image as displayed in Fig. 6(a). While local maxima of the ODoB output are directly used as initial seeds, no new seeds are created while expanding the regions. Prior this step, the user is able to determine a free-form *Region of Interest (ROI)* in order to exclude bogus regions

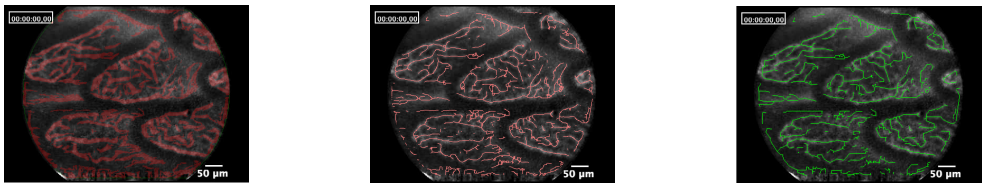

(a) (b) (c)

Figure 6: Results of rough vessel detection: (a) segmented regions obtained by *Seeded Region Growing* and (b) the corresponding morphological skeletons; (c) the resulting forest of *Minimum Spanning Trees* after *Split-and-Merge* simplification.

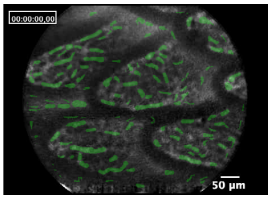

(a) sampled vessel areas from input image 3(a)

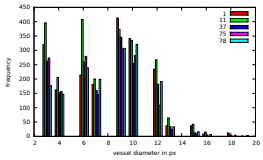

(b) distribution of vessel diameters for five distinct frames from the same image sequence

Figure 7: Sampled vessel areas used for further statistical computations.

from onward processing as well as to adjust the amount of objects regarded as foreground, *i.e.* the number of seeds for SRG. Finally, the user is able to delete wrong objects or to close gaps between segmented areas.

After segmenting the foreground hypotheses, their *morphological skeletons* already give initial approximations of the vessel axes, as depicted in 6(b). These skeletons are obtained by morphological closing operations iteratively repeated as long as not more than the middle line of an object remains. By computing these skeletons, the still unrelated foreground pixels are augmented by a neighborhood structure. Since vessels can split into parts, *i.e.* one vessel might dissolve into several sub-vessels, hierarchical relations can be obtained in an optimal way by concepts taken from *graph theory*. Therefore, we transform the skeleton points into *weighted graph trees* $\mathcal{G} = (E, V, w)$ of edges E and directed vertices V with associated weights w. These graphs are further decomposed into a forest of *Minimum Spanning Trees (MST)*. In order to remove degenerated trees and to reduce the number of branches along the vessels, we further simplify the MSTs in a *Split-and-Merge* way. Using these tree branches, the final vessel boundaries are obtained for each pixel located at the vessel axes, as shown in Fig. 6(c). As a further chance for feedback, we allow the user to manually select vessel endpoints in order to include missed structures. An optimal path through the graph is obtained by applying Dijkstra's algorithmemploying a cost function based on locally enhanced ODoB filter outputs.

3 Statistical Vessel Analysis

Given the detected vessel structure, we are able to derive a couple of statistics in order to assist the diagnosis after endomicroscopic imaging. One key characteristic of mucosal microvascularization is the distribution of vessel diameters within the examined region. Since vessels might intersect, overlap, or occlude each other, those vulnerable regions should not be

Table 1: Average runtimes of individual steps in our approach.

Process Step	Elapsed Time
ODoB filtering	0.491 s
Seeded Region Growing	0.028 s[1]
Minimal Spanning Tree	1.284 s
Split-and-Merge Simplification	0.047 s

[1] per iteration

Table 2: Overview of statistical parameters derived from our final segmentation of Fig. 3(a).

Parameter	Symbol	Value
Total vessel length	l_{vessel}	8633 µm
Total vessel area	A_{vessel}	29773 µm^2
Total ROI area	A_{ROI}	109369 µm^2
Mean vessel diameter	$\mu(d_{\text{vessel}})$	8.2432 µm
Vessel diameter std. dev.	$\sigma(d_{\text{vessel}})$	3.4339 µm
Relative vessel area	$A_{\text{FCD}} = \frac{A_{\text{vessel}}}{A_{\text{ROI}}}$	27.222522
Number of branches	N_{B}	158
Fractal dimension	D	1.827129
Lacunarity	Λ	0.152779

taken into account for further analysis. To overcome this problem, we draw representative samples from the vessel tree (*cf*. Fig. 7(a)) to approximate the distribution of vessel diameters. Fig. 7(b) exemplarily shows this histogram obtained for the image given in Fig. 3(a). In order to compare or match histograms obtained from different frames or to monitor changes over time in delayed recordings, we calculate the intra and inter class distances as well as the *Earth Mover's Distance (EMD)* of extracted vessel diameter histograms. These provide a very robust similarity measure. Beyond this histogram, several other statistical or form-describing parameters are obtained, as summarized in Tab. 2.

4 Evaluation & Discussion

The proposed system was implemented in `C++` using the parallelization toolbox `OpenMP` and tested on a desktop computer equipped with a Intel Core-i7 CPU running at 3.4 GHz and 16 GB of RAM. ODoB filters for all orientations are precomputed and stored into a look-up table after start-up. As display in Tab. 1, all processing steps are able to perform very fast. Hence, the user interaction steps shape the bottleneck.

Since ground truth data is rarely available for our test data, we show exemplary results to evaluate the performance of the proposed framework qualitatively. Considering the images shown in Fig. 8 one can see that our system creates accurate segmentation from CLE images. It benefits from the early integration of prior knowledge during ODoB-filtering. Misdetections can be strained off by further plausibility considerations.

5 Summary & Outlook

We presented a framework to process, segment, and analyze CLE images of mucosal vascularisation with minimal user interaction. For this purpose, we introduced *Oriented Differences of Boxes* filters as combined non-linear smoothing and derivation operators to simultaneously suppress noise and enhance local structure. Further processing steps include *Seeded Region Growing* for foreground segmentation, morphological skeletonization, construction of *Minimum Spanning Trees*, and *Split-and-Merge* simplification. In a preliminary clinical study it was shown that our approach provides excellent results and performs in real-time. The statistical parameters we obtained were successfully verified by experts. Moreover, we are

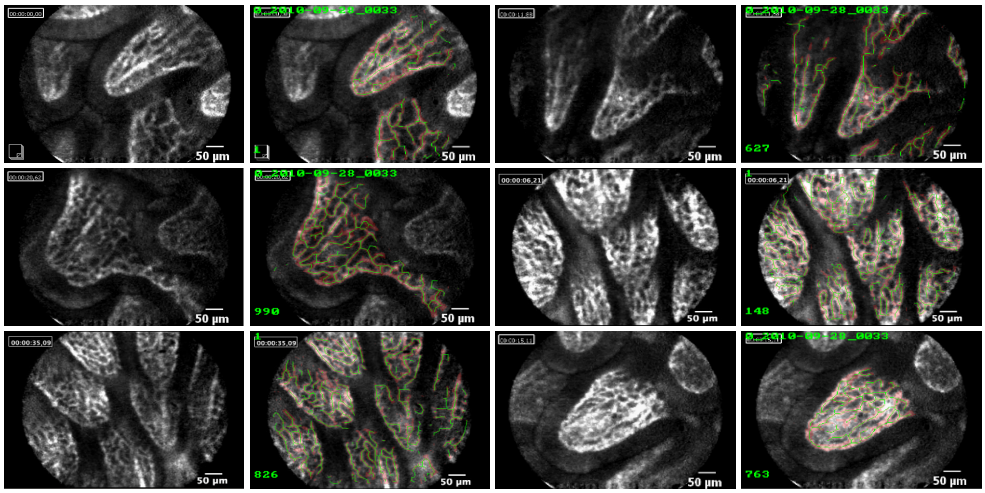

Figure 8: Exemplary results of our approach. Odd columns: original porcine *ileum* CLE images, even columns: segmented vessel structure (red) and obtained trees (green).

currently evaluating the applicability of this algorithm for the evaluation of other imaging modalities in gastroenterology and cardiology, *e.g*. images obtained by endoscopic retrograde cholangiopancreaticography and coronary angiography, respectively.

References

[1] R. Adams and L. Bischof. Seeded region growing. *TPAMI*, 16(6):641–647, 1994.

[2] D. Lesage, E. D. Angelini, I. Bloch, and G. Funka-Lea. A review of 3d vessel lumen segmentation techniques: Models, features and extraction schemes. *MIA*, 13(6):819–845, 2009.

[3] D. Paulus, S. Chastel, and T. Feldmann. Vessel segmentation in retinal images. *SPIE Medical Imaging*, pages 696–705, 2005.

[4] E. Rodner, H. Süße, W. Ortmann, and J. Denzler. Difference of boxes filters revisited: Shadow suppression and efficient character segmentation. In *Document Analysis Systems*, pages 263–269, 2008.

[5] Y. Rouchdy and L.D. Cohen. Retinal blood vessel segmentation using geodesic voting methods. In *ISBI*, pages 744–747, 2012.

[6] R. Socher, A. Barbu, and D. Comaniciu. A learning based hierarchical model for vessel segmentation. In *ISBI*, pages 1055–1058, 2008.

[7] L. Xu and S. Luo. A novel method for blood vessel detection from retinal images. *BioMedical Engineering OnLine*, 9(1):14, 2010.

[8] Y. Zheng, H. Wang, J. Wu, J. Gao, and J.C. Gee. Multiscale analysis revisited: Detection of drusen and vessel in digital retinal images. In *ISBI*, pages 689–692, 2011.